DESIGN AND DEVELOPMENT OF A DUAL OPERATING MODE MICROSTRIP PATCH ANTENNA FOR UNMANNED AERIAL VEHICLE SYNTHETIC APERTURE RADAR

P. N. Tan, T. S. Lim*, V. Gobi, and Y. K. Chan**

Faculty of Engineering & Technology, Multimedia University, Jalan Ayer Keroh Lama, Bukit Beruang, Melaka 75450, Malaysia

Abstract—Microstrip patch antenna has been designed and developed for Unmanned Aerial Vehicle based Synthetic Aperture Radar (UAVSAR). This antenna operates in C-Band at the frequency of 5.3 GHz with a bandwidth of 80 MHz. The radiation patterns of the antenna were specified to provide a desired scanned area for UAVSAR. The UAVSAR antenna was designed in the form of combination of 3 subpanels to allow dual operating mode (single antenna or dual antenna) selection. Two feed points are provided to the feeding network of each subpanel to reduce undesired power loss. The developed antenna prototype meets the performance requirements of UAVSAR system. It shows promising results in the UAVSAR flight mission conducted in Mersing area, Malaysia for both operating modes.

1. INTRODUCTION

Since the first system developed in 1922 by Taylor [1], radar has been widely utilized for various purposes such as military defense system, air traffic control system and remote sensing [2]. Remote sensing is the science of obtaining data and information of features, objects and classes on earth surface without any physical contact [3]. Synthetic Aperture Radar (SAR) is classified as active remote sensing as it is able to operate day or night, in all-weather condition. SAR operates in microwave frequency band and can penetrate cloud and even forest canopy.

The first airborne SAR was developed in 1953, by Goodyear research facility in Arizona, where a wide beamwidth (100°) Yagi-uda antenna was applied and operated at 930 MHz [1]. With the

advancement of microwave technology, civilian SAR systems operated at higher frequency such as L-band, C-band and X-band. Horn antenna and slotted waveguide antenna became the most popular antenna for SAR applications until microstrip patch antenna took over to become the dominant choice of SAR antenna.

Dual band [3] and dual polarization airborne SAR antennas have been achieved in recent SAR antenna development. However, typical airborne SAR antenna normally operates at only single antenna mode or dual antenna mode but not both. In other words, an airborne SAR antenna operates at single antenna mode is impossible to integrate with a dual antenna mode airborne SAR system and vice versa.

Starting from the year 2009, Multimedia University in collaboration with Remote Sensing Agency of Malaysia, developed an UAVSAR system. It is a single vertically polarized, pulse radar system operating at 5.3 GHz (C-band). The UAVSAR antenna is able to operate at both single antenna and dual antenna modes by adjusting the coaxial cables feeding network configuration. Table 1 shows some selected specification of the UAVSAR.

2. AIRBORNE SAR ANTENNA CONSTRAINTS

Different from conventional antenna, SAR antenna faces several electrical design constraints, in addition to the mechanical design limitations of the carrier platform. The electrical design constraints are also known as SAR ambiguities. The ambiguities can be classified into three types, namely "Azimuth Ambiguity", "Range Ambiguity", and "Left-right Ambiguity". In addition, as most of the airborne SAR systems implement side-looking scan method, "Range Gain Variation" correction is needed to compensate the difference of delivered power in range due to large scanned area.

Table 1. Design specification of UAVSAR.

Mode of Operation	Stripmap
Altitude	1 km
Incident Angle	30°
Swath Width	525 m
Azimuth Beamwidth	3°
Elevation Beamwidth	24°
Platform Speed	30 m/s
Pulse Repetition Frequency (PRF)	640 Hz

The flight of SAR sensor across ground target area will result in Doppler frequency shift proportional to the relative velocity of the target and a time delay proportional to range. The azimuth signals will experience aliasing in the frequency domain due to the sampling rate of the pulse. Targeted band in the main lobe will be corrupted due to this aliasing signal and cause ambiguity. Azimuth ambiguity can be quantified by computing the ratio of total aliasing signal over the main beam signal, which is known as azimuth ambiguity over signal ratio (AASR) [4]. Typically, maximum AASR is set to $-20\,\mathrm{dB}$. It can be calculated through the formula stated as below [5]:

$$
\text{AASR} = \frac{\sum\limits_{\substack{m=-\infty \\ m\neq 0}}^{\infty} \int\limits_{-B_P/2}^{B_P/2} G^2(f + mf_r) dF}{\int\limits_{-B_P/2}^{B_P/2} G^2(f) dF}, \tag{1}
$$

where f represents the operating frequency, f_r is the pulse repetition frequency, G represents the gain and B_P represents the azimuth processing bandwidth.

Range ambiguity occurs when the previous echo signal returns to the SAR system receiver after the next pulse signal has been transmitted. Airborne SAR systems are not affected by range ambiguity due to the low altitude. In this SAR sensor, the PRF is $640\,\mathrm{Hz}$ and the slant range is only $2.691\,\mathrm{km}$.

For most of the ground mapping radars especially side looking airborne SAR system with wide beamwidth, a challenging issue is the existence of gain variation at near range and far range. It is due to the
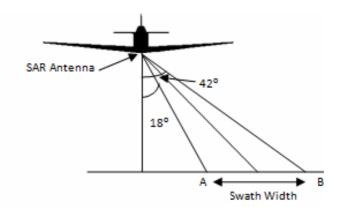

Figure 1. Range gain variation.

difference between the distance from near range target and far range target to the SAR sensor. An example of range gain variation is shown in Figure 1 where the near range target (A) has a higher reflected signal as compared to the far range target (B). To avoid this problem, the antenna gain pattern is shaped accordingly and the shaped pattern is commonly known as "cosec-squared" pattern [6].

Left right ambiguity refers to the inability of the SAR system to differentiate return signal from left side or right side of the SAR sensor platform as the return time from left side or right side of the SAR sensor platform are similar [7]. It might result in inaccuracy of the SAR image and the solution to overcome this issue is to suppress the antenna sidelobe [8]. Figure 2 shows an example of left right ambiguity where the unwanted target located at the left side of the UAV might introduce error to the output of the SAR sensor.

With the SAR system constraints in mind, the E-plane of the SAR antenna is designed to have a "cosec-squared" pattern from $18°$ to $42°$ with a beamwidth of $24°$ and look angle of $30°$. The normalized sidelobe level of the E-plane radiation pattern should be kept below -15 dB. For H-plane, a pencil beam will be adopted with beamwidth of $3°$ and the sidelobe level shall be kept below -20 dB.
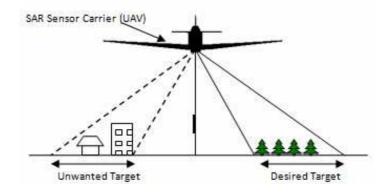

Figure 2. Left right ambiguity.

Table 2. Effects of radius of hole on ground plane to performance of reflection coefficient.

Radius of hole (mm)	1.00	1.25	1.50	1.75	2.00
Reflection Coefficient at 5.3 GHz (dB)	-28.3	-23.9	-21.5	-20.3	-19.5

3. MICROSTRIP PATCH ANTENNA

In this antenna, three layers are utilized with the feeding network located at third layer behind the ground plane and radiating element located at top layer. This will help to reduce spurious feed radiation and offer flexibility in feeding network design. Glass reinforced hydrocarbon and ceramic laminates (RO4003C by Rogers Corp) is selected to be the substrate for this antenna. Ansoft Designer EM simulation tool is utilized to simulate the performance of the antenna. Rectangular patch is selected with the patch dimension of 13.8 mm in length and 15 mm in width. 70 Ohms feedline is adopted in this antenna to obtain line width of approximately 2 mm to reduce spurious radiation from the feedline, this feedline is then transformed
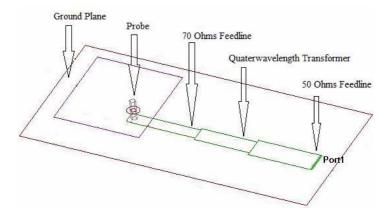
Figure 3. Geometry structure of single patch microstrip patch antenna.

Figure 4. Fabricated single patch microstrip patch antenna.

to 50 Ohms by using a microstrip quaterwavelength transformer then only connected to the SMA connector. The feed point is offset 2.3 mm from center point of the patch to achieve optimum reflection coefficient. The feeding network is connected to the patch via a probe with a hole created at the ground plane with the size of 1 mm to avoid contact of the ground plane with the probe.

The radius of the hole located at the ground plane might influence the performance of reflection coefficient of the antenna. Based on simulation result shown on Table 2, it is obvious to observe that the value of reflection coefficient of the antenna will increase to certain level with the increase of radius of hole. However, an over small radius might introduce mutual coupling of the probe with the ground plane. Therefore, the radius of hole in this antenna is chosen to be 1 mm.

Figure 3 shows the geometry structure of single patch microstrip patch antenna while Figure 4 shows the fabricated single patch antenna. The performance of the single patch antenna is then measured to compare with the simulation result. The comparison of simulation and measurement results is shown in Figure 5 and Table 3. The difference of simulation and measurement result is possibly due to
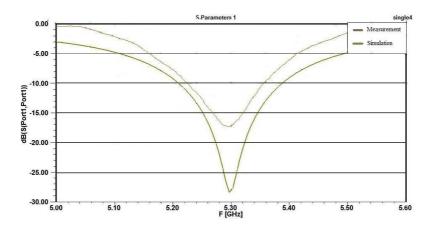

Figure 5. Comparison of simulation and measurement reflection coefficient of single patch antenna.

Table 3. Comparison of simulation and measurement results.

	Simulation	Measured
Operating Frequency	5.3 GHz	5.3 GHz
Reflection Coefficient	−28	−17.8
Bandwidth	175.6 MHz	166 MHz

uneven or oversized of radius of the hole located at ground plane. In this simulation, the radius of the hole is 1 mm in this antenna which creates a gap of 0.5 mm from the ground plane to the feeding probe. However, the in-house fabricated microstrip single patch antenna could suffer from oversized or uneven circle. Larger radius of the hole will worsen the performance of the reflection coefficient and cause a higher reflection loss.

4. MICROSTRIP PATCH ARRAY

The array is made up of 24 elements in the azimuth plane and 6 elements in the elevation plane. The array is then divided into a smaller group which consists of 8 azimuth elements and 6 elevation elements to form the subpanel. Hence it allows the UAVSAR to operate in single antenna and dual antenna mode which will be discussed in later part of this paper.

The required specification is achieved with the use of 6 radiating elements spaced 0.53λ apart. Woodward-Lawson method is applied in the array synthesis. An elevation beamwidth of $24°$ with look angle of $30°$ away from nadir and maximum nominal sidelobe level of $-15\,$dB is achieved. The excitation coefficient is shown in Table 4.

A feeding network is designed to distribute the power and adjust the phase shift of each radiating elements. In order to reduce power dissipation due to the extremely long transmission line, the feeding network is split into two half, which is connected through a 2-way 3 dB power divider. The EM power is distributed to each radiating element by utilizing a microstrip T-junction power divider integrated in the feeding network and $70\,\Omega$ microstrip transmission line is adopted as main transmission line. The microstrip T-junction dividers distribute the EM power according to the preset relative excitation amplitude. The power distribution ratio is shown in Figure 6 while Figure 7 shows the layout of the elevation feeding network.

In the azimuth plane, a pencil beam array with beamwidth of $3°$ and with maximum sidelobe level of $-20\,$dB is designed. A uniform array with 24 elements spaced 0.7λ apart is used to achieve this pattern. The feeding network is constructed with parallel feeding method and T-junction power divider is connected.

Table 4. Excitation coefficients of elevation plane array.

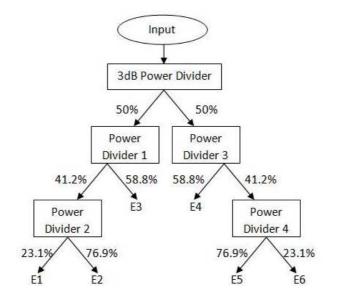| Element No.	1	2	3	4	5	6
Relative Amplitude	1	3.33	6.17	6.17	3.33	1
Phase (Degree)	285	229	326	214	311	255

Figure 6. Power distribution of the elevation feeding network.

Figure 7. Layout of the elevation feeding network.

The E-plane array and H-plane array are combined to form a planar array. The planar array consists of total number of 144 radiating elements with 6 rows of 24 patches each and the antenna's dimension is approximately 1 meter in length and 0.30 meter in width. The antenna is divided into 3 sub panels and each panel consists of 48 radiating elements with 6 rows of 8 patches each. Since each sub panels consists of 2 feeding ports, hence there will be a total 6 feeding ports for the complete antenna. A 6 way power divider will be utilized to combine all the feeding ports to the RF section. The complete layout of the feeding network is shown in Figure 8. Figure 9 shows the complete antenna formed by the 3 antenna panels. The supporting structure was made of aluminum to ensure durability and light weight.
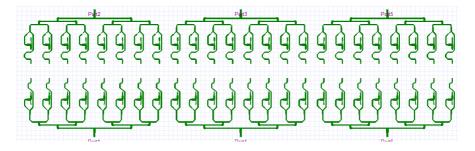
Figure 8. Layout of feeding network of complete antenna.

Figure 9. Complete antenna with supporting structure.

5. MEASUREMENT RESULT

The antenna's radiation pattern for H-plane and E-plane are measured in the Anechoic Chamber. In Figure 10, the H-plane radiation pattern shows a peak sidelobe of -18 dB located at $20°$. The sidelobe levels below $-30°$ and above $30°$ are below -20 dB.

The E-plane radiation pattern is measured with the far field region of $\frac{2D^2}{\lambda}$ or approximately 35.3 meters. As shown in Figure 11 the E-plane radiation pattern is shown as below with a peak sidelobe of -15 dB located at $-60°$ to $-65°$. The discrepancy of the measured and simulated sidelobe level might be due to inaccuracy of power delivered to each of the radiating elements. The undesired return echo received from the sidelobe located at $-60°$ to $-65°$ can be filtered by the RF section. The sidelobe located at $-20°$ to $-40°$ with normalized gain of -17.5 dB will reduce possible undesired return echo from the opposite of the scan area. Besides, the antenna shows a good reflection loss of -32.381 dB at 5.3 GHz as shown in Figure 12.

The antenna is then integrated with the SAR sensor on a truck to perform ground test. The SAR system scanned the target area as the truck is driven through with the antenna mounted on the side of the truck. This ground test measurement simulates the motion of the

airborne SAR and then produce an image of the scanned area. The processed image of test site showing multiple natural targets detected at more than 1km away from the SAR sensor. The result proves the capability of the SAR sensor and antenna to produce image of the scanned area.
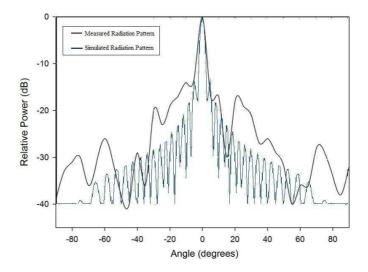

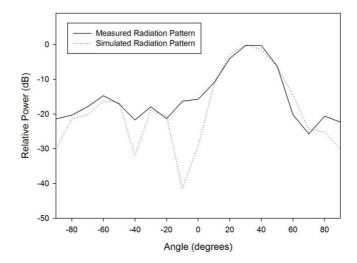**Figure 10.** *H*-plane radiation pattern.
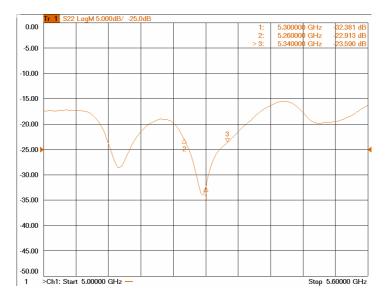

Figure 11. *E*-plane radiation pattern.

Figure 12. Reflection coefficient of the complete antenna.

Figure 13. Mounting location of the antenna to the UAV.

6. SINGLE ANTENNA OPERATION

On Oct. 2010, the airborne SAR system was tested on an Unmanned
Aerial Vehicle (UAV) in Semporna, Sabah. The antenna was installed
underneath the UAV as shown in Figure 13. Figure 14 shows the
comparison of processed image and respectively Google Earth image of
the same test site. The processed image shows strong signal reflection
from the buildings of the scanned area, comparison to the Google Earth
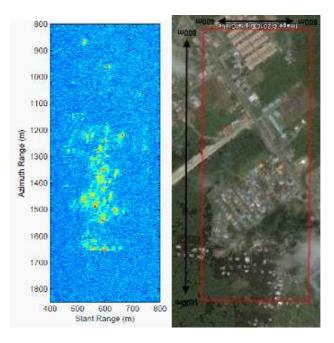
Figure 14. Comparison of SAR image using single antenna and google earth image.

image. However, ground objects with lower reflection coefficient cannot be seen in the image as the single antenna SAR system suffers from high leakage from the circulator.

7. DUAL ANTENNA OPERATION

Single antenna operation mode suffers from high leakage from the circulator. Thus, to improve the quality of the image, the SAR antenna was reconfigured as a dual antenna system. Two of the antenna's sub panels were used as the transmitting and receiving antennas. The middle panel was terminated in a matched load to avoid any reflections. The elevation radiation pattern of the dual antenna system remained unchanged while the azimuth beamwidth will be increased to 5°.

In Dec 2010, the dual antenna mode UAVSAR system was tested on same platform again, but in a different location (Mersing, Johor). Figure 15 below shows the SAR images processed from the captured data during the flight measurement, with comparison of Google Earth image of the same site. Clear signatures of river, roads, forest and urban can be observed from the SAR images.
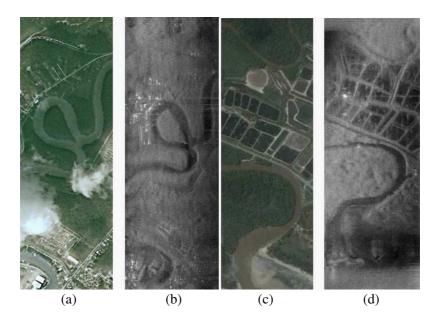
(a) (b) (c) (d)

Figure 15. (a), (c) Google earth image of scan areas. (b), (d) SAR images using dual antenna system.

8. CONCLUSION

A microstrip patch antenna has been developed, and the performance of the antenna is verified by indoor and outdoor measurements. The possibility of selection of single antenna or dual antenna operating mode enables the UAVSAR to operate with either mode without changing the UAVSAR antenna. Meanwhile, low sidelobe level of the antenna eliminates left-right ambiguity which is a common constraint for airborne SAR and allows the UAVSAR to produce a better quality SAR image. The ground and flight measurements results prove the durability and functionality of the antenna as an UAVSAR antenna.

ACKNOWLEDGMENT

REFERENCES

1. Chan, Y. K. and V. C. Koo, "An introduction to synthetic aperture radar (SAR)," *Progress In Electromagnetic Research B*, Vol. 2, 27–60, 2008.

2. Skolnik, M. I., *Introduction to Radar Systems*, McGraw Hill, Singapore, 2001.

3. Islam, M. F., M. A. M. Ali, B. Y. Majlis, and N. Misran, "Dual band microstrip patch antenna for SAR applications," *Australian Journal of Basic and Applied Sciences*, Vol. 4, No. 10, 4585–4591, 2010.

4. Chan, Y. K., B.-K. Chung, and H.-T. Chuah, "Transmitter and receiver design of an experimental airborne synthetic aperture radar sensor," *Progress In Electromagnetics Research*, Vol. 49, 203–218, 2004.

5. Curlander, J. C. and R. N. McDounough, *Synthetic Aperture Radar, Systems and Signal Processing*, John Wiley & Sons, New York, 1991.

6. Besso, P., M. Crozzoli, D. Forigo, and R. Vallauri, *Design and Characteristics of a Sector/Cosec2 Shaped Beam Microstrip Antenna*, Antennas and Propagation Conference Publication, No. 407, 85–88, 1995.

7. Christensen, E. L. and M. Dich, "SAR antenna design for ambiguity and multipath suppression," *International Symposium on Geoscience and Remote Senssing*, Vol. 2, 784–787, 1993.

8. Vetharatnam, G., B. K. Chung, and H. T. Chuah, "Design of a microstrip patch antenna array for airborne SAR applications," *Journal of Electromagnetic Waves and Applications*, Vol. 19, No. 12, 1687–1701, 2005.